

ORIGINAL PAPER OPEN ACCESS

Energy-Aware Protocol Design and Evaluation of the PHY Layer in Satellite IoT

Simon Heine  | Christian A. Hofmann | Andreas Knopp

Institute of Information Technology, University of the Bundeswehr Munich, Bavaria, Germany

Correspondence: Simon Heine (papers.sp@unibw.de)**Received:** 18 June 2024 | **Revised:** 15 November 2024 | **Accepted:** 12 December 2024**Funding:** This research paper is funded by dtec.bw - Digitalization and Technology Research Center of the Bundeswehr. dtec.bw is funded by the European Union - NextGenerationEU.**Keywords:** direct-to-satellite | energy efficiency | low power wide area networks | non-terrestrial networks | physical layer | protocol design | satellite iot | spectral efficiency

ABSTRACT

Direct-to-satellite communication for the Internet of Things (IoT) has attracted significant interest from both the scientific community and major telecommunications players. The integration of satellite connectivity in smartphones and IoT devices promises a transformative impact on critical applications such as environmental monitoring, asset tracking, agriculture, and nature conservation. These applications require reliable and energy-efficient technologies for transmitting sensor data from regions without terrestrial networks, necessitating robust design of waveforms and protocols. This work investigates the most suitable IoT protocols for direct-to-satellite communication, emphasizing overhead, spectral, and energy efficiency. By introducing a framework and evaluation metrics that incorporate physical layer overhead into the evaluation, a comprehensive analysis of the effective energy efficiency in satellite IoT systems is conducted. Our findings highlight substantial differences among the Low Power Wide Area Network (LPWAN) protocols. Consequently, we propose a new classification for the most energy-efficient protocols, termed Massive Multiple Access very Low Power Wide Area Networks (MMA-vLPWANs). This classification aims to streamline the selection process for energy-conscious satellite IoT waveforms for deployments in remote areas. The results not only advance the understanding of protocol efficiency in satellite IoT communications but also offer a guideline for optimizing power usage in IoT devices, extending their operational life and enhancing their utility in inaccessible regions.

1 | Introduction

Digital connectivity has become increasingly widespread and sophisticated around the world, offering every industry fertile ground for enhanced efficiency and innovation. According to current projections, the number of connected Internet of Things (IoT) devices will increase to 34.7 billion by 2028 [1]. The IoT becomes a key enabler of entirely new applications in mobility, healthcare, manufacturing, logistics, and retail promising a boost of the global gross domestic product (GDP) by \$1.2 trillion to \$2 trillion until 2030 due to higher connectivity [2]. Moreover, as the demand for data continues to grow, the energy

consumption of the communication infrastructure will also increase, resulting in even greater environmental impacts.

Industrial communication solutions have been realized primarily through cellular standards such as EC-GSM-IoT, LTE Cat M1, Narrowband-IoT (NB-IoT), and low power wide area networks (LPWAN) such as LoRaWAN or Sigfox. Indisputably, new communication technologies for industrial purposes play a decisive role in the standardization of the 3rd Generation Partnership Projects (3GPPs). By seeking global connectivity in regions where cellular coverage is not provided, Release 17 of 3GPP standardization extends the fifth generation (5G) of

This is an open access article under the terms of the [Creative Commons Attribution](https://creativecommons.org/licenses/by/4.0/) License, which permits use, distribution and reproduction in any medium, provided the original work is properly cited.

© 2024 The Author(s). *International Journal of Satellite Communications and Networking* published by John Wiley & Sons Ltd.

cellular networks by incorporating non-terrestrial networks (NTN) for the first time [3]. As new research initiatives in the scientific community already focus on the sixth generation (6G) of the cellular standard, the question of what role NTN will play in this context arises [4]. Early publications propose multilayered communication networks to be integrated in the third dimension combining different types of network and system architectures, as an integral part of 6G [5]. In this context, data transmission via satellites attracts data transmission via satellites attracts attention from researchers and start-ups alike. In addition to the development of mega constellations in LEO to provide high-rate broadband services on earth [6, 7], the number of partnerships between cellular providers and satellite operators has increased. Recent examples are the cooperations between Apple and Globalstar [8], T-Mobile and SpaceX [9] or Vodafone and AST SpaceMobile [10]. In addition, microchip manufacturers such as Qualcomm are seeking cooperation with satellite constellation operators to actively shape the development of next-generation semiconductors [11]. The aim of these collaborations is to enable smartphones to connect to non-terrestrial communications services to provide emergency communications services. As these are battery-powered handheld devices with narrow system constraints, deploying efficient transmission technologies is essential for enabling connectivity to the satellite. Likewise, emerging ventures increasingly focus on industrial use cases of satellite IoT constellations, in particular offering M2M communication services [12] aiming to occupy new business fields through applications in digital agriculture, smart manufacturing, healthcare, or environmental monitoring. Tangible services like wildlife monitoring [13, 14] become feasible through satellite communications in terms of higher cost-effectiveness and connectivity provision over large distances and across borders. Tracking animal movements using non-terrestrial space infrastructure on a global scale provides unforeseen insights into the state of the natural environment, animal populations, and the impact on human health. In this context, knowledge about animal migration routes is fundamental for analyzing the cause and spread of infectious diseases that are critical for humans, such as the severe acute respiratory syndrome SARS-CoV-2 (coronavirus disease COVID-19), which was found to be spread by bats, including its transfer to humans [15].

The areas of application shown in Figure 1 can be categorized under the term Internet of Remote Things (IoRT), which according to [16] is understood as intelligent remote objects distributed over a wide geographical reference. Consequently, the accelerated expansion and scaling of New Space IoT constellations [17–19] offering these services demand for an increased provision of technical resources. The construction, commissioning, operation, and maintenance of a satellite constellation impact significantly on the environment [20]. Researchers studying the impact of modern space launches see the emission of various aerosols associated with the expansion of infrastructure in space as an increasing threat to our planet. Especially the climate response is proportional to the increase in emissions from rocket launches over time where even modest black carbon injections cause sensitive reactions of the stratosphere [21]. Based on these early insights, the question arises whether the construction of a large number

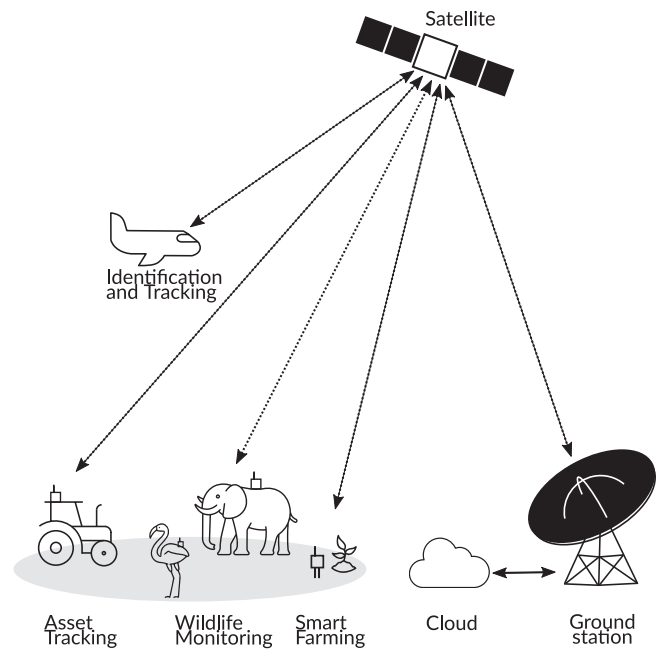


FIGURE 1 | Direct-to-satellite IoT scenario presenting exemplary application cases under battery constraints where energy-optimized communication concepts are vital.

of satellite constellations accompanied by an increasing number of launches is requisite or if it is more advisable to utilize existing systems and resources in space in combination with new communication technologies.

With a focus on sustainable system design, research already presents investigations addressing problems of energy efficiency, power consumption, or data storage. The bottleneck in power supply of IoT data-gathering gateways of geodistributed IoT networks which use LEO satellite constellations as transport network is addressed by the authors of [22]. On the space segment, the authors of [23] analyze on-board battery consumption during inter-satellite communication in LEO satellite constellations and proposing a contact plan design for a store-and-forward approach to optimize delivery of data and utilization of battery. With regard to direct-to-satellite communication the implementation of efficient and reliable transmission technologies becomes the core aspect to be solved in the IoRT. Of particular interest are compact-sized, battery-powered, and remotely accessible IoT transceivers [24, 25]. An exemplary direct-to-satellite IoT scenario under these conditions is illustrated in Figure 2. IoT sensors or actuators that are independent of terrestrial networks, installable everywhere, independent on orbit height, and consuming as little power as possible will be the source of vast amounts of information in the future.

Hence, this work is led by a central theme imposing the following requirements on the IoT system: We investigate IoT protocols for **small, lightweight, and low-cost** devices that offer reduced **battery power** consumption and **worldwide connectivity**, which can be deployed at **scale** in a **highly mobile** environment and in large quantities, independent of any terrestrial infrastructure. Publications of recent years have addressed the topic of

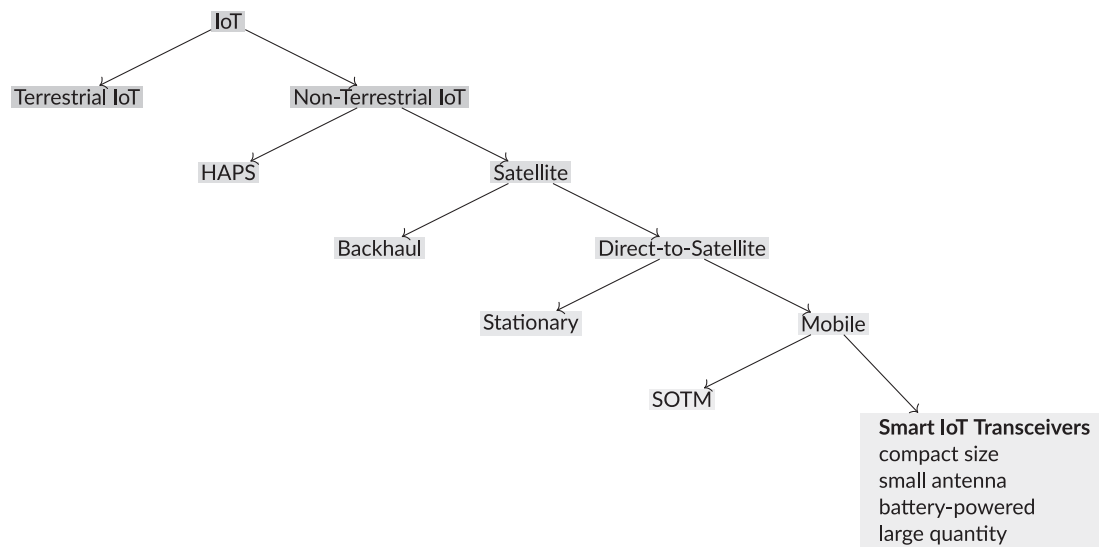


FIGURE 2 | Positioning of this work within the IoT field, highlighting its focus on ultra-low power satellite IoT waveforms specifically designed for energy-constrained transceiver hardware.

direct-to-satellite IoT from a variety of perspectives, such as system architecture [26, 27], multiple access [28, 29], or potential applications [30, 31]. However, the issue of transmission energy efficiency has yet received little scientific attention. By focusing on a specific scenario in this paper, we aim to contribute to the understanding and selection of energy-efficient IoT protocols to complement research in direct-to-satellite communication.

The considered application scenario results in various technological constraints that must be met by the particular used communication technology. A small, lightweight, and affordable IoT solution implies a transceiver design with **minimum transmission power**, almost **zero antenna gain**, and **low-priced components**. Devices with hard power restrictions for battery operation must build on highly energy-efficient communication protocols incorporating only a **minimum of overhead**. Technical challenges imposed by the satellite constellation itself, such as **Doppler shift**, **latency**, and **fading**, have to be mitigated by the communication technology. As the considered IoT device should be scalable in quantity, not solely the production price is relevant but also the capability to efficiently use the scarce spectrum. Therefore, the IoT technology requires a high robustness against interference from other devices or services and an efficient and reliable multiple access scheme. In the further course of this paper, we refer to this set of criteria as the Massive Remote Battery-powered (MaReBa) IoT scenario. A result of this vision is the question of the ideal transmission technology for space-related IoT services [32].

Throughout this work, we build on these restrictions to evaluate the applicability of existing IoT waveforms to satellite communication. There exists a variety of suitable approaches in industry and in research for a direct-to-satellite application. Transmission technologies such as those currently being integrated by Apple, Starlink, AST SpaceMobile, or short message services from existing operators such as Galileo or Beidou, fit into our defined scenario. For our analysis, we restrict ourselves to nonproprietary protocols that offer a sufficient basis of publicly available information for a performance comparison. Further, we exclude

an investigation of protocols within the 3GPP standard due to their increased overhead and complexity in connection establishment. Based on our review of protocols, we propose the introduction of a new IoT class, termed Massive Multiple Access very Low Power Wide Area Networks (MMA-vLPWAN), which meets the requirements of the emerging IoT application field in the MaReBa scenario.

The main contributions of this paper are the following:

- We provide a mathematical foundation of performance metrics to evaluate IoT protocols in the scope of spectral and energy efficiency. A new evaluation metric named effective energy efficiency accounting for the protocol overhead is introduced.
- We perform a detailed in-depth analysis of selected IoT protocols suitable for direct-to-satellite communication by applying the previously introduced methodology.
- We compare and judge the selected IoT protocols in terms of energy and spectral efficiency and compare their suitability for application in GEO and LEO systems.
- We identify and define MMA-vLPWAN as a new class of IoT, which is best suited to the requirements of very low-power satellite IoT. This classification is integrated into the broader landscape of communication protocols, where it is distinguished from other waveforms by its core properties.

The remainder of this paper is structured as follows. A direct-to-satellite IoT scenario and practical performance metrics with emphasis on power constraint IoT transceivers are introduced in Section 2. Section 3 briefly presents IoT physical (PHY) layer standards qualified for the purpose of satellite IoT communication. In Section 4, we analyze the introduced IoT standards for application in a satellite scenario with respect to spectral and energy efficiency. In Section 5, we resort to the introduction of a new class of IoT. The paper is concluded in Section 6.

2 | Satellite IoT System Model

This section provides a generic system model for the return link of satellite IoT. The model builds upon the considerations of the previously described satellite IoT scenario, mapping them into appropriate metrics for performance measurements.

2.1 | Protocol Efficiency

The communication overhead of a protocol has a decisive influence on the efficiency and power consumption of a communication system. Especially in the context of MaReBa IoT, the overhead at the PHY and MAC layers constitutes a significant portion of the energy consumed when transmitting a fixed payload. Therefore, a precise definition of the metrics within the system model is essential. In the following, we introduce a generic protocol structure model (Figure 3) that incorporates standard elements common to most satellite-compatible IoT protocols.

Let p denote the user payload in bits, specifically defined as the scalar value representing the number of bits that comprise the message of the user. The parameter p serves as the starting point for calculating the total packet or frame length, $L_{fr,n}(p)$, for a given protocol n . This notation highlights that p represents the bit count rather than any specific data content. Further, we refer

to the actual bit stream of the payload as the “user bits”. Figure 3 illustrates the overhead components (scalars) contributing to total packet length as,

- header and tail information for PHY (h_{phy} , h_{phy_tail}) and MAC (h_{mac} , h_{mac_tail}) layer,
- preambles (h_{pre}), pilots (h_{pilot}), or midambles (h_{mid}),
- authentication (h_{auth}),
- cyclic redundancy checks (CRC) (h_{crc}),
- message counters (MC) (h_{mc}),
- header replicas (h_h), or packet replicas (h_{rep}),
- and integrated control channels (h_{pccr}).

The block diagram in Figure 4 shows the communication chain to form a transmit signal where the blocks on sender side represent components of the system that add overhead to the user bits. The protocol-specific overhead appended to the user bits is accounted by the dashed left block of the graphic. We quantify the amount of overhead by the payload ratio $R_{p,n}(p)$, which is a factor that measures the relative number of payload bits within a single frame of a specific protocol. While forward error correction (FEC) also adds overhead, we keep it separate from the payload ratio for clarity, representing it as $R_{c,n}$ in the formula.

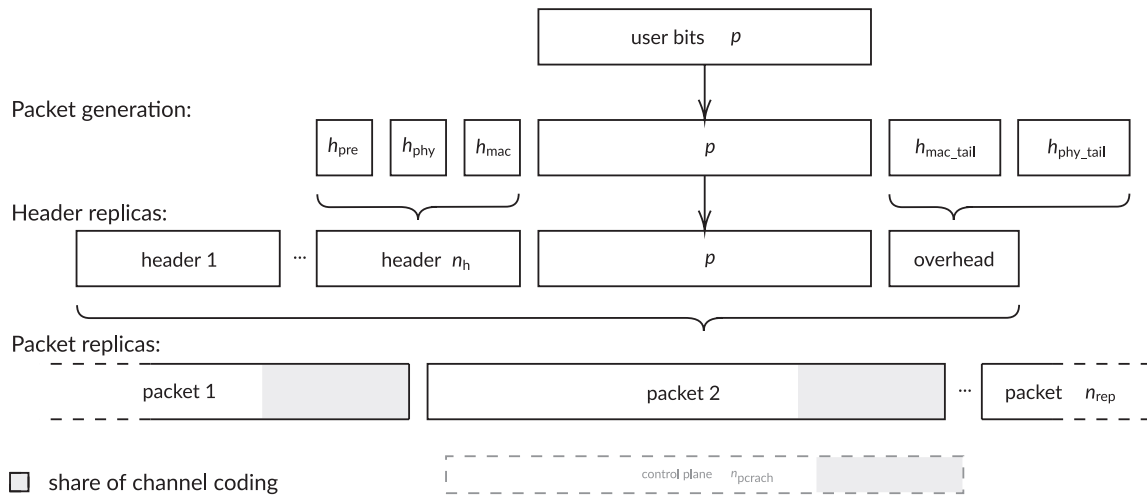


FIGURE 3 | Generic protocol structure for uplink communication from the IoT device including visualization of forward error correction overhead as line pattern.

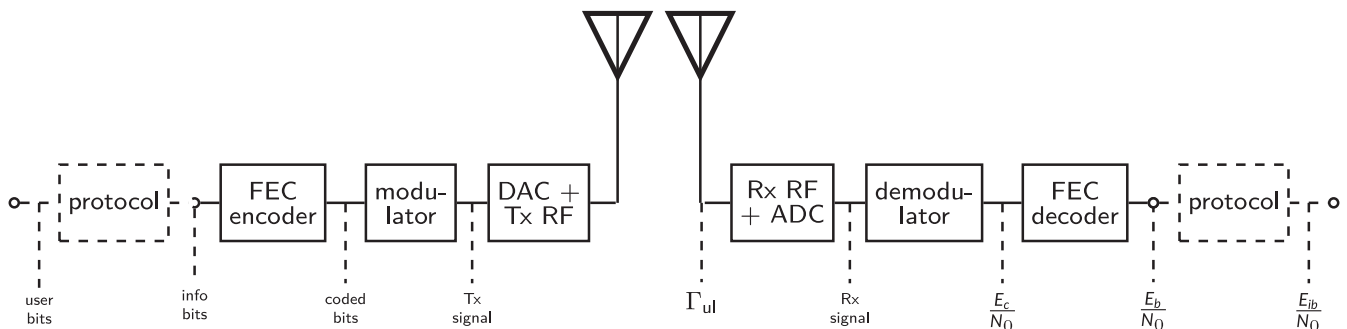


FIGURE 4 | General block diagram of an IoT communication model including metrics and definitions used in this paper.

This separation allows flexibility, as many protocols offer multiple FEC code rates to choose from. Combining $R_{p,n}(p)$ and $R_{c,n}$ in the calculation, we express the total packet length $L_{fr,n}(p)$ as follows:

$$L_{fr,n}(p) = \frac{1}{R_{c,n}} \cdot \frac{1}{R_{p,n}(p)} \cdot p. \quad (1)$$

Since each IoT protocol composes payloads, headers, and replicas in different ways, the payload ratio is meant to condense this overhead information dependent on the chosen user payload. Thereby, we consider overhead of the physical and the MAC layer, whereby a clear differentiation to the following higher layer is not always possible. The calculation of the payload ratio for the individual protocols is presented in the following section.

2.2 | Spectral Efficiency

The spectral efficiency is among the major indicators for performance evaluation of PHY layer communication technology and therefore an inevitable measure for the selection of appropriate candidates in direct-to-satellite IoT. The spectral efficiency η in bit/s/Hz describes the data rate that can be achieved within a given bandwidth B in a particular communication system as

$$\eta_n = \frac{R_{b,n}}{B}, \quad (2)$$

where $R_{b,n}$ is the achievable information bit rate of protocol n , which should be understood as the net bit rate

$$(\text{net rate})_n \leq (\text{gross rate})_n \cdot R_{c,n} \quad (3)$$

excluding redundant coding overhead. On the other hand, the gross bit rate describes the total amount of physically transferred bits per second through the wireless channel. The spectral efficiency is dependent on the selected transmission technology of the IoT protocol which in turn distorts comparability by adding overhead. Consequently, we have to define an overhead adjusted effective spectral efficiency by multiplying the previously defined payload ratio as

$$\eta_{\text{eff},n}(p) = R_{p,n}(p) \cdot \eta_n \quad (4)$$

for a defined user payload size p . The resulting effective spectral efficiency in true user-bit/s/Hz thus holds as a novel metric for a fair comparison of IoT protocols.

2.3 | Energy Efficiency

We take the discussion of IoT standards in satellite communication a step further by addressing the energy efficiency. Comparative metrics as the energy per bit to noise power spectral density E_b/N_0 require a link budget with focus on the user uplink of the return channel toward the satellite. This communication link is the limiting and primarily critical factor due to constraint transmission power of the battery-powered IoT device regarded as the originator of communication in the system. We consider M

IoT devices, transmitting simultaneously within a transmission time frame $[t_k, t_{k+1}]$. The m -th IoT device with $m \in \{1, 2, \dots, M\}$ transmits the signal $x_m(t)$ with transmit power $P_{tx,m}$ in dBW using an antenna with gain $G_{tx,m}(\epsilon)$ in dBi dependent on the elevation angle ϵ where tx denotes the transmit side. The effective isotropic radiated power (EIRP) in dBW is then given by

$$P_{\text{eirp},m}(\epsilon) = P_{tx,m} + G_{tx,m}(\epsilon). \quad (5)$$

Neglecting interference, the link budget between IoT device and satellite in the uplink is described by the signal-to-noise ratio (SNR) in dB at the receiver given by

$$\Gamma_{ul}(\epsilon) = P_{\text{eirp},m}(\epsilon) - L_{\text{fsp}}(\epsilon) - L_{\text{att}} + G_s(\epsilon) - T_{\text{noise}} - 10\log_{10}\{k\} - 10\log_{10}\{B\}, \quad (6)$$

where L_{att} groups atmospheric effects as rain attenuation, polarization loss, ionospheric loss, and others. Further, G_s stands for the satellite antenna gain, T_{noise} is the noise temperature of the satellite side, k is the Boltzmann constant, and B is the bandwidth. In addition, L_{fsp} stands for the free space path loss (FSPL) and is defined by

$$L_{\text{fsp}}(\epsilon) = 10\log_{10}\left\{\left(\frac{4\pi d(\epsilon)f_c}{c}\right)^2\right\}, \quad (7)$$

where f_c denotes the carrier frequency, $d(\epsilon)$ marks the slant range as a function of ϵ , and c stands for the speed of light. The slant range between IoT user terminal and satellite is given by

$$d(\epsilon) = \sqrt{r_e^2 \sin^2(\epsilon) + a + 2r_e a - r_e \sin(\epsilon)} \quad (8)$$

where r_e is the Earth radius and a is the satellite altitude measured from the Earth's surface.

In the case of a GEO satellite, ϵ changes only with the location of the IoT device, whereas in the LEO case, ϵ is mainly dependent on the trajectory of the satellite by an inversely proportional relationship as

$$\epsilon \rightarrow \min(\epsilon) \geq 0: d \rightarrow \max(d) \quad (9)$$

and

$$\epsilon \rightarrow \max(\epsilon) \leq 90^\circ: d \rightarrow \min(d), \quad (10)$$

leading to a variable loss in the link budget, due to a longer slant path through the atmosphere [33]. In consideration of the required SNR Γ_{req} at the satellite receiver to ultimately close the communication link, the achievable data rate R_b in the bandwidth B lies within the proportionality to the required energy per bit to noise power spectral density $(E_b/N_0)_{\text{req}}$ by

$$\Gamma_{\text{req}} = \left(\frac{E_{b,\text{req}}R_b}{N_0B}\right)_{\text{req}} = \eta \cdot (E_b)_{\text{req}}. \quad (11)$$

We compare IoT protocols by the ratio of required energy per coded bit to noise power spectral density E_c/N_0 , the E_b/N_0 of

uncoded bits, and the E_{ib}/N_0 of solely information bits (user bits). For this purpose, a localization of the metrics within the system model is illustrated in Figure 4. Consequently, the protocol-specific evaluation of the E_b/N_0 is defined as

$$(E_{ib})_n = (E_b)_n - 10\log_{10}\{R_{p,n}(p)\} \quad (12)$$

in dB by adjusting the required E_b/N_0 values with the previously defined payload efficiency $R_{p,n}(p)$. Further, we compute back to the necessary EIRP emitted by an IoT device to reach the required $(E_b/N_0)_{\text{req}}$ at the receiver, via the previously classified satellite link budget in (6). The energy efficiency ξ in bit/Joule as described in [34] and [35] quantifies the amount of bits that can be transmitted per unit of energy. We obtain

$$\{\xi_n\}_{\text{bit/Joule}} = \frac{\{R_{b,n}\}_{\text{bit/s}}}{\{P_{\text{eirp},n}\}_W} \quad (13)$$

from the required P_{eirp} and the achievable data rate R_b of protocol n . Accordingly, we adjust the energy efficiency by the payload ratio of user bits transmitted to define the effective energy efficiency as

$$\{\xi_{\text{eff},n}\}_{\text{user-bit/Joule}} = \{\xi_n\}_{\text{bit/Joule}} \cdot R_{p,n}(p). \quad (14)$$

Consequently, ξ_{eff} enables the comparison of IoT protocols in the MaReBa scenario.

3 | IoT Standards Suitable for Satellite Communication

This section provides an overview of wireless protocols and standards suitable for IoT satellite communication, fitting to the use case of small remote battery-powered devices. In this regard, we focus on the first two layers of the OSI model, the PHY, and the MAC layer.

3.1 | LoRa

LoRa names the physical layer of the low-power wide-area network (LPWAN) technology based on a proprietary chirp spread spectrum (CSS) modulation licensed by the company Semtech. LoRaWAN defines the MAC layer of the LPWAN applying ALOHA type random access for all users to minimize the complexity of the network and maximize energy savings [36]. The LoRaWAN protocol has been examined for use in space communication considering the adapt-ability of the standard [37], multiple access [38], or ionospheric scintillation [39].

For our comparison, we develop a mathematical abstraction of the IoT packet structure, which allows us to quantify the code rate $R_{c,\text{lor}}a$ and payload ratio $R_{p,\text{lor}}a(p)$ separately. We only consider LoRaWAN Class A for uplink communication in the satellite-based IoT scenario.

The length of a LoRa packet in symbols is calculated as

$$L_{\text{fr},\text{lor}}a(p) = (h_{\text{pre},\text{lor}}a + 4.25) + L_{\text{pld},\text{lor}}a(p), \quad (15)$$

where $h_{\text{pre},\text{lor}}a = 8$ are the first preamble symbols followed by a 4.25 symbol long SyncWord. The length of the payload in symbols as defined in [40], for explicit header mode, is

$$L_{\text{pld},\text{lor}}a(p) = 8 + \max \left(\left\lceil \frac{28 + 8L_{\text{mac}}(p) + 16b_{\text{crc}} - 4n_{\text{sf}} - 20b_{\text{h}}}{4(n_{\text{sf}} - 2b_{\text{de}})} \right\rceil (n_{\text{cr}} + 4), 0 \right), \quad (16)$$

where L_{mac} is the number of PHY payload in bytes, b_{crc} is a Boolean variable with $b_{\text{crc}} = 1$ if present and $b_{\text{crc}} = 0$ if absent. The number $n_{\text{sf}} \in \{7, \dots, 12\}$ stands for the spreading factor which is the amount of raw bits that can be encoded by a symbol. The Boolean b_{de} indicates whether low data rate optimization is used ($b_{\text{de}} = 1$) or not ($b_{\text{de}} = 0$). The definition of the explicit header mode is defined opposite, indicating the header enabled with $b_{\text{h}} = 0$ and not enabled with $b_{\text{h}} = 1$. In this review, we consider explicit header mode and low data rate optimization as enabled. Further, $n_{\text{cr}} \in \{1, \dots, 4\}$ specifies the coding rate defined as

$$R_{c,\text{lor}}a = \frac{4}{n_{\text{cr}} + 4}. \quad (17)$$

Besides, we consider the detailed composition of the MAC layer frame within the PHY payload L_{MAC} as

$$L_{\text{mac}}(p) = h_{\text{mhdr}} + h_{\text{fhdr}} + h_{\text{fport}} + p + h_{\text{mic}} \quad (18)$$

with h_{mhdr} summarizing a fixed 8bit MAC header and h_{fhdr} stands for the frame header containing device address, frame control, frame counter, and optional frame options for MAC commands. The message integrity code is stored in the 32 bit long h_{mic} field; further, the 8 bit h_{fport} field indicates that the user payload field p is not empty. Hence, the maximum available user payload $p_{\text{max},\text{lor}}a$ calculates depending on flexible frame options and regional LoRaWAN PHY layer specifications [41]. For our scenario, we do not transmit frame options ($h_{\text{fhdr}} = 7$ byte) and use the lowest data rate classified as DR0 = 250bit s⁻¹ with spreading factor $n_{\text{sf}} = 12$ in the EU863-870 ISM Band, and maximum user payload $p_{\text{max},\text{lor}}a = 51$ byte. Conclusively, we can compute the payload ratio by converting (1), introduced previously, for the LoRa protocol as

$$R_{p,\text{lor}}a(p) = \frac{p}{n_{\text{sf}} \cdot R_{c,\text{lor}}a \cdot L_{\text{fr},\text{lor}}a(p)}, \quad (19)$$

where the amount of user payload bits is translated into symbols by division of the spreading factor.

3.2 | LoRa Frequency Hopping Spread Spectrum

The LoRaWAN protocol specification RP002-1.0.2 [42] of 2020 introduces a new waveform called LoRa Frequency Hopping Spread Spectrum (LR-FHSS). LR-FHSS increases network capacity and robustness significantly and is thus traded as enabling technology for new applications including communication via satellites. The waveform was analyzed regarding packet delivery and network scalability for a direct-to-satellite case, showing support for devices that transmit infrequently (every 15 min) [43].

LR-FHSS implements the ability to frequency modulate the uplink by a fast frequency hopping technique which increases interference resistance and reduces packet collisions. A data packet is split into fragments of 50 ms in length which are transmitted in randomly selected subchannels of 488 Hz within the total bandwidth of 137 and 336 kHz or 1.523 MHz. The frequency hopping pattern is stored in the LR-FHSS packet header changing the carrier frequency every 102.4 ms for the payload fragments and every 233.472 ms for the PHY-layer header. Resulting data rates of LR-FHSS are 162bit s⁻¹ for 1/3 payload coding rate and 325bit s⁻¹ for 2/3 payload coding rate.

The 114 byte long LR-FHSS header composes as

$$h_{\text{lrfhss}} = h_{\text{syncword}} + 2 \cdot (h_{\text{phdr}} + h_{\text{phdr-crc}}) + 2 \quad (20)$$

where the SyncWord h_{syncword} is 4 byte in length, h_{phdr} and $h_{\text{phdr-crc}}$ are 4 byte, respectively, 1 byte long and coded with a fixed FEC rate of 1/2, followed by a 2-bit-long pause. The full protocol structure in bits of LR-FHSS is then

$$L_{\text{fr,lrfhss}}(p) = \frac{p + h_{\text{crc}}}{R_{\text{c,lrfhss}}} + (h_{\text{lrfhss}} \cdot n_{\text{h}}), \quad (21)$$

where $R_{\text{c,lrfhss}}$ is the coding rate separately applied to the number of user bits p and the 2-byte CRC. Additionally, the header h_{lrfhss} is sent up to $n_{\text{h}} = 4$ times to further improve the robustness of the modulation against in-band interference. The resulting payload ratio for LR-FHSS yields to

$$R_{p,\text{lrfhss}}(p) = \frac{p}{p + h_{\text{crc}} + n_{\text{h}} R_{\text{c,lrfhss}} h_{\text{lrfhss}}}. \quad (22)$$

Further, both modulation types, LoRa and LR-FHSS, can co-exist and be modified by downlink ADR commands from the network server.

3.3 | Sigfox

Sigfox is a French telecommunications operator developing a proprietary, global wireless IoT network [44]. The technology defines the PHY and the MAC layer of the communication protocol stack. Signal modulation is noncoherent by applying differential binary phase shift keying (DBPSK) to encode symbol information in the phase difference between adjacent signals. On the MAC layer, Sigfox makes use of a random access method comprising triple diversity namely in space, frequency, and time domain. Sigfox packet is sent three times on random frequencies and at random time intervals. Further, a Sigfox device is not assigned to a certain base station, leading to an average reception of a message by circa three base stations nearby. To the best of the authors' knowledge, the Sigfox standard has not been investigated for space communication from a research perspective. On the business side, Sigfox partnered up with Eutelsat in 2018 for the Eutelsat LEO for Objects (ELO) satellite constellation to better analyze the satellite ISM spectrum and to process data from IoT devices [45].

The full Sigfox frame structure in bits assembles to

$$L_{\text{fr,sig}}(p) = \frac{h_{\text{mac}} + 8[p/8] + h_{\text{auth}}(p) + h_{\text{crc}}}{R_{\text{c,sig}}} + h_{\text{phy}} \cdot n_{\text{rep}}, \quad (23)$$

where for coding, $R_{\text{c,sig}}$ is either 1 or 1/3, defining bit interleaving and single resp. triple packet transmission. Therefore, $n_{\text{rep}} = 1/R_{\text{c,sig}}$ ensures to account for the correct number of header bits if packet repetitions are considered. The authentication field $h_{\text{auth}}(p)$ takes values from 2 to 5 byte dependent on the user payload and defined in a lookup table in the specification [46]. The CRC field h_{crc} is 16 bit long. Further, the 6-byte fixed MAC header h_{mac} is a sum of

$$h_{\text{mac}} = h_{\text{li}} + h_{\text{bf}} + h_{\text{rep}} + h_{\text{mc}} + h_{\text{id}} \quad (24)$$

with length indicator (h_{li}), bidirectional frag (h_{bf}), repeated flag (h_{rep}), message counter (h_{mc}), and identifier (h_{id}), respectively. We summarize the PHY header as

$$h_{\text{phy}} = h_{\text{pre}} + h_{\text{ft}}, \quad (25)$$

where the uplink preamble h_{pre} is 19 bit long and the frame type (h_{ft}) is 13 bit long. Hence, we calculate the payload ratio for the subsequent comparison as follows:

$$R_{p,\text{sig}}(p) = \frac{p}{h_{\text{mac}} + 8[p/8] + h_{\text{auth}} + h_{\text{crc}} + h_{\text{phy}}}. \quad (26)$$

3.4 | Telegram Splitting Ultra-Narrowband

Telegram Splitting Ultra-Narrowband (TS-UNB) is a patented transmission technology developed by the German Fraunhofer IIS institute, also known under its brand name MIOTY. The technology is designed for the use in terrestrial LPWANs for commercial and industrial IoT applications [47]. However, Fraunhofer IIS successfully tested the utilization of TS-UNB without any special adaptations for GEO satellite communication. In the test setup, the stations transmitted directly to the EchoStar XXI communications satellite in S-band at 2 GHz [48].

The PHY layer of TS-UNB builds up on (Gaussian) Minimum Shift Keying (MSK) signal modulation and ultra-narrowband telegram splitting for random channel access. During radio transmission, data packets are split into tiny burst sequences which are spread over time and frequency domain. Consequently, TS-UNB achieves higher robustness against interference allowing the receiver to still decode entire packets irrespective of lost transmission bursts. From a network perspective, devices are grouped into Class Z (only uplink) and Class A (bidirectional) with respective protocol characteristics [49]. Downlink communication is implemented to be only activated by a preceded uplink transmission. TS-UNB is capable to send up to 245 bytes of application data in uplink and up to 250 bytes in downlink; however, the protocol is optimized for a user payload of 10 bytes, which marks the core framework of the protocol. The developers claim that more than 1.5 million messages per day per base station in a 200 kHz wide frequency band can be handled [50].

The full frame format of TS-UNB is formulated as

$$L_{\text{fr,tsunb}}(p) = \left(\frac{p + h_{\text{tsunb}}}{R_{\text{c,tsunb}}} + h_{\text{tail}} \right) \cdot n_{\text{split}}, \quad (27)$$

where $R_{\text{c,tsunb}}$ stands for the code rate, h_{tail} is a 18bit long tail, and $n_{\text{split}} = 1.5$ is the splitting factor accounting for an additional pilot sequence within the final transmission bursts. All remaining fixed header bits with a total length of 104 bits combine as

$$h_{\text{tsunb}} = h_{\text{mac-hdr}} + h_{\text{address}} + h_{\text{mpducnt}} + h_{\text{mpf}} + h_{\text{sign}} + h_{\text{crc-hdr}} + h_{\text{crc-pyld}} + h_{\text{psi}} + h_{\text{mmode}}, \quad (28)$$

with a 16 bit long address and without setting the flag of the MAC Payload Format (MPF) field. The resulting payload ratio is then

$$R_{p,\text{tsunb}}(p) = \frac{p}{(p + h_{\text{tsunb}} + R_{\text{c,tsunb}}h_{\text{tail}}) \cdot n_{\text{split}}}. \quad (29)$$

3.5 | Enhanced Spread Spectrum ALOHA

Enhanced Spread Spectrum ALOHA (E-SSA) is an asynchronous random access scheme which is part of the standard of the air interface for the S-band Mobile Interactive Multimedia (S-MIM) system [51]. We choose E-SSA, among other RA schemes for satellite networks [28], due to its unslotted nature which is more suitable to the presented IoT scenario. Further, E-SSA is designed for a large volume of user terminals in the M2M and IoT segment with emphasis on the high performance of the return link employing asynchronous spread spectrum Aloha (SSA) techniques for multiple access. The waveform of the return link originates from a modified version of the 3GPP Wideband Code Division Multiple Access (W-CDMA) Standard Random Access Channel (RACH) physical layer design [52]. The detector is central to the system as it provides reliable detection of incoming packets even in the presence of high MAC channel utilization and random power distribution of packets. It utilizes iterative successive interference cancellation (iSIC) adapted to the asynchronous random access direct-sequence (DS) spread spectrum (SS) scheme [53].

The structure of an E-SSA frame is defined by the Physical Data Random Access Channel (PDRACH) and the Physical Control Random Access Channel (PCRACH) which are I/Q code multiplexed and preceded by a preamble h_{pre} to form an uplink burst. The frame size in bits calculates as

$$L_{\text{fr,essa}}(p) = h_{\text{pre}} + \frac{h_{\text{pdrach-hdr}} + 416 \lceil p/416 \rceil + h_{\text{crc}}}{R_{\text{c,essa}}} + h_{\text{uw}} + h_{\text{pcrach}}, \quad (30)$$

where the 64bit PDRACH header $h_{\text{pdrach-hdr}}$, the 416bit user payload p , the 16-bit CRC h_{crc} , and the 36-bit long unique word (UW) h_{uw} compose the PDRACH frame with a total length of 1536 bits (coding with $R_{\text{c,essa}}$ included). The PCRACH frame h_{pcrach} accordingly states the same length containing a sequence of pilot symbols supporting channel estimation for coherent detection. Based on (1) we calculate the resulting payload ratio as follows.

$$R_{p,\text{essa}}(p) = \frac{p}{R_{\text{c,essa}} \cdot L_{\text{fr,essa}}(p)}. \quad (31)$$

3.6 | Unipolar-Coded Chirp Spread Spectrum

Unipolar-coded spread spectrum (UCSS) is an IoT-waveform published by Hofmann et al. in 2019 [54, 55]. UCSS is imagined for energy-efficient satellite communication even in C-band and above for distributed small transceivers taking advantage of low data rates of a few bit/s. The authors demonstrated a closing link between a GEO satellite and a handheld IoT transmitter utilizing the UCSS waveform. The technology makes use of a unipolar-coded form of CSS and random multiple access for a large number of devices. Therefore, a Zadoff-Chu sequence, respectively, constant amplitude auto-correlation (CAZAC) chirp sequence is multiplied for spectrum spreading resulting in a spreading gain proportional to the length of the chirp sequence [54]. Data blocks are encoded by a FEC code and modulated by applying differential binary phase shift keying (DBPSK).

Regarding the impact of phase noise on the waveform, UCSS has been compared to the CSS waveform LoRa [56]. In comparison, UCSS performs better in terms of robustness against linear frequency drifts, which is a significant performance factor for transmission in ultra-narrowband.

For estimating frame length and overhead of UCSS, we calculate the number of symbols spent for preamble, payload, and pilots from the theory given in [56]

$$\begin{aligned} L_{\text{fr,ucss}}(p) &= \frac{T_{\text{fr,ucss}}(p)}{T_s} = \frac{T_{\text{pre}}}{T_s} + \frac{T_{\text{pl}}(p)}{T_s} + \frac{T_{\text{pause}}(p)}{T_s} \\ &= n_{\text{pre}} + n_{\text{pl}}(p) + \frac{\lceil n_{\text{pl}}(p)/2 \rceil^2}{n_{\text{sf}}}, \end{aligned} \quad (32)$$

where $T_{\text{fr,ucss}}$ is the total time of an UCSS frame with symbol duration T_s . Further, UCSS transmits $n_{\text{pre}} = 6$ preamble symbols within the time T_{pre} . The symbols accounting to the overall payload are transmitted within $T_{\text{pl}}(p) = T_s \cdot n_{\text{pl}}(p)$, with n_{pl} defined as

$$n_{\text{pl}}(p) = \frac{p + h_{\text{crc}}}{R_{\text{c,ucss}}}, \quad (33)$$

where the user payload p in bits, a CRC h_{crc} of 16 bits, a code rate of $R_{\text{c,ucss}} = 1/2$ is specified and random multiple access for a large number of devices, by introducing short pause times between the symbols. The length of all UCSS pause intervals is given by

$$T_{\text{pause}}(p) = \lceil n_{\text{pl}}(p)/2 \rceil^2 / R_s, \quad (34)$$

where R_s stands for the sample rate which provides us the symbol duration $T_s = n_{\text{sf}}/R_s$ and is used for the relation in (32). Since UCSS uses DBPSK modulation, we can translate symbols directly to bits in the subsequent comparison. Hence, the payload ratio can be formulated as

$$R_{p,\text{ucss}}(p) = \frac{p}{\frac{R_{c,\text{ucss}} T_{\text{pre}}}{T_s} + p + h_{\text{crc}} + \frac{R_{c,\text{ucss}} T_{\text{pause}}(p)}{T_s}}. \quad (35)$$

3.7 | Narrowband IoT

Narrowband Internet of Things (NB-IoT) is a LPWAN standard developed by 3GPP for cellular devices and services. Introduced in Release 13 of LTE-Advanced Pro, NB-IoT is specifically designed to meet the requirements of low data rate machine-type communications, offering improved cost and power efficiency by reducing complex signaling overhead associated with traditional LTE systems. With the increasing importance of global connectivity, integrating support for NTN, such as satellite connectivity, into 3GPP standards has become a high priority. Starting from Release 17, 3GPP specifications included normative requirements for NTN, making it possible to gradually incorporate satellite support within the NB-IoT ecosystem. In the subsequent Release 18, 3GPP distinguished between two satellite connectivity components: IoT-NTN (supporting NB-IoT/eMTC satellite access) and NR-NTN (supporting NR satellite access). NB-IoT can be deployed in three distinct modes: standalone (utilizing GSM or satellite spectrum), guardband (between LTE carriers), or in-band (within LTE resource blocks). The uplink transmission employs Single-Carrier Frequency Division Multiple Access (SC-FDMA) with subcarrier spacing options of 15kHz or 3.75kHz. Key physical layer components include the Narrowband Demodulation Reference Signal (DM-RS), Narrowband Physical Uplink Shared Channel (NPUSCH), and Narrowband Physical Random Access Channel (NPRACH) [57].

For data transmission, we assume the utilization of NPUSCH format 1, whereby the payload and the CRC are encoded by a turbo encoder. To enhance error resilience, a dedicated rate matching block is applied, followed by channel interleaving. It is assumed that no additional overhead is introduced through these steps. Subsequently, scrambling is applied, followed by modulation, which is limited to the formats $\pi/2$ -BPSK and $\pi/4$ -QPSK, both of which are employed for single-tone transmissions, and QPSK, which is used for multitone transmissions [58]. These modulation formats were selected by the standard to achieve a reduced peak-to-average power ratio (PAPR), which in turn results in lower power consumption. Given the highly constrained nature of our scenario, we assume that the IoT device transmits utilizing format 1, with a subcarrier spacing of 3.75kHz and $\pi/2$ -BPSK modulation, as this configuration leads to the highest robustness [57]. The frame length, measured in bits, for an NB-IoT data transmission can be approximated by

$$L_{\text{fr},\text{nb-iot}}(p) = \frac{p + h_{\text{crc}}}{R_{c,\text{npusch}} \cdot R_{\text{npusch}_\text{nprach}}}, \quad (36)$$

where h_{crc} represents the 24-bit CRC and $R_{c,\text{npusch}}$ denotes the turbo encoder rate of 1/3. Additionally, we consider NPRACH as an additional overhead, as its preamble consists of a single tone that does not carry useful information. We define

$$R_{\text{npusch}_\text{nprach}}(p) = \frac{t_{\text{npusch}} \cdot (p + h_{\text{crc}})}{t_{\text{nprach}} + t_{\text{npusch}} \cdot (p + h_{\text{crc}})} \quad (37)$$

as the overhead ratio introduced by the NPRACH channel, providing a high-level approximation of the primary overhead influence in NB-IoT. For simplicity, we exclude minor influences, such as DM-RS. We assume a single packet transmission with one NPRACH and one NPUSCH occurrence. For NPRACH, we assume preamble format 1 with a preamble duration of 6.4 ms, since format 1 has a longer cyclic prefix compared to format 0, which facilitates the detection of the preamble at the eNB. We assume 32 preamble retransmissions, as suggested in [59] for a NTN scenario, leading to a total preamble duration t_{nprach} of 204.8ms. Although up to 64 retransmissions are possible, such a high number would significantly impact overhead efficiency, hence we adopt the best-case of [59]. Although retransmissions are feasible, we consider only a single packet transmission during NPUSCH occasion. Here, t_{npusch} represents the duration of a bit in NPUSCH (0.286 ms), assuming a slot of 7 symbols with a duration of 2 ms, given 3.75 kHz of subcarrier spacing and $\pi/2$ -BPSK modulation. The resulting payload ratio is then

$$R_{p,\text{nb-iot}}(p) = \frac{p}{(p + h_{\text{crc}}) \cdot \frac{1}{R_{\text{npusch}_\text{nprach}}}}. \quad (38)$$

3.8 | Satellite IoT Waveforms Open for Investigation

In the course of our research, we identified further waveforms developed for deployment in direct-to-satellite IoT. These waveforms are still in their infancy or are not published with sufficient details to provide enough data for our comparison; although, they still offer valuable starting points for further investigations in the MaReBA IoT scenario:

Folded Chirp-Rate Shift Keying (FCrSK) is a modulation technique proposed by [60] based on CSS with improvements in handling Doppler effects compared to LoRa. Simulation shows that FCrSK outperforms LoRa in terms of large Doppler shifts while staying slightly below LoRa performance without Doppler shifts.

The company Totum Labs aims to build a LEO IoT constellation deploying their patented waveform Doppler Multi-Channel Spread Spectrum (DMSS) [61]. DMSS addresses technological challenges of satellite IoT, as Doppler shift robustness, indoor coverage, respectively, indoor location, and high capacity of simultaneous transmissions [62]. A technology demonstrator payload that was launched to space successfully established an indoor-to-satellite link [63].

For M2M communication networks via GEO satellites, Supervisory Control and Data Acquisition (SCADA) systems have been developed, using types of Scrambled Coded Multiple Access (SCMA) or Interleaved Division Multiple Access (IDMA) to provide low data rate connections and multiple user access. A simulation of a spread SCMA scheme showed the applicability for 64 users transmitting QPSK symbols at 220bit s⁻¹ with 1/15 code rate in a 31.25kHz width GEO S-band channel [64]. The technology does not require complex power control as small low-cost user terminals utilizing power amplifiers with not more than 15dBm realize long battery lifetimes. Further investigations on SCMA technology prototypes have been made by the satellite service provider Hughes [65].

The ICARUS system, a joint project of the Max Planck Institute of Animal Behavior, the German Aerospace Center (DLR), and the Russian aerospace agency Roscosmos, is developed for wildlife monitoring under a non-terrestrial approach for data transmission [14]. The communications payload is installed on the International Space Station (ISS) collecting position data from animals equipped with miniature IoT tags as it passes overhead. The IoT tag with a volume of about 2 cm³ and a weight of less than 5 g equipped with a microcontroller and several integrated sensors is typical for the type of IoT deployed within the MaReBa scenario. The communication technology utilizes various phase shift keying (PSK) modes for modulation and a code division multiple access (CDMA) scheme for channel access on a licensed carrier frequency of 401 to 406 MHz. The ICARUS technology achieves a net data rate of 520 bit s⁻¹ within a bandwidth of 1.5 MHz transmitting 1784 data bits per overhead pass [66]. ICARUS is designed for operation in LEO fleets, where the ISS acts as an initial test platform. The expansion of the system to a constellation at a later point in time could increase availability and reduce overflight intervals.

4 | Comparison of Protocols Suitable for Satellite IoT

This section compares the previously introduced candidates for satellite IoT communication on three different stages regarding effective information throughput, spectral efficiency,

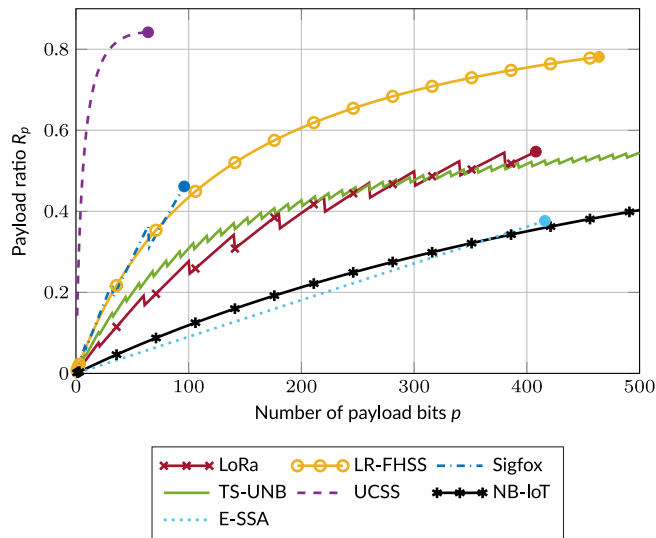


FIGURE 5 | Portion of user bits per packet (payload ratio) $R_{p,n}$ of a single packet of protocol n as function of the user payload p .

and energy efficiency. The following assumptions are applied for the comparison:

- Focus on uplink transmission from a remote battery-powered sensor device to a satellite.
- No estimation of the wireless transmission channel.
- Limitation to the PHY and MAC layers of protocols.
- No consideration of package acknowledgments or retransmission schemes.

4.1 | Overhead Comparison on Protocol Level

For an initial evaluation of protocol efficiency, we propose a simple mathematical model in (1) of Section 2 consisting of the multiplicative ratios $R_{c,n}$ and $R_{p,n}(p)$ which stand for the code rate and the payload ratio, respectively. Both ratios provide insight into the number of overhead bits ultimately appended to the user payload for packet construction of a satellite IoT protocol. For a fair comparison of protocols, this assessment is indispensable, since each overhead bit results in additional energy consumption during transmission. The ultimate goal should be to use the most overhead efficient protocol possible to improve communication with a satellite.

A general indication for the impact of overhead for a given payload presents Figure 5 plotting the calculated payload ratio $R_{p,n}(p)$ starting from one payload bit up to the maximum number of user bits per packet. The maximum possible payload lengths are marked with a filled circle at the end of the curve with the exception of TS-UNB and NB-IoT which support up to 245 and 317 byte user payload not fitting reasonably into the plot. Further, some curves show tiny spikes and edges in their progression, which result from fixed protocol fields where fractions of bytes are rounded up to the next full byte.

We recognize UCSS as already very efficient for small user payloads and LR-FHSS, assuming three header replicas, as an efficient protocol for larger payloads. Further, from the linear course of E-SSA, the fixed payload size of 416 bits can be recognized, which leads to the optimal payload ratio with full utilization. The associated payload ratios are widely varying, as they include many protocol-specific features such as header retransmissions. However, the share of payload usually accounts for more than 40%. We notice that three of the protocols have similar maximum user payload sizes of 51 to 58 bytes; the remaining protocols rank below that, including TS-UNB, since it is optimized for 10 user bytes according to the specification but can support a maximum of 245 user bytes payload. NB-IoT is an exception in

TABLE 1 | Overview code rates R_c and maximal payload ratios $R_{p,max}$ for the maximum user payload p_{max} in byte.

	LoRa	LR-FHSS	Sigfox	TS-UNB	UCSS	NB-IoT	E-SSA
Code rate R_c	4/5 4/6 4/7 4/8	1/3 2/3	1/3	1/3	1/2	1/3	1/3
Payload $\{p_{max}\}_{byte}$	51	58	12	245	8	317	52
Payload ratio $R_{p,max}$	0.55	0.78	0.46	0.63	0.84	0.77	0.38

regard to payload, since 3GPP Release 14 the maximum number of bits per transmission in NPUSCH was increased from 1000 to 2536 bits (317 byte).

Note, $R_{p,n}(p)$ solely considers overhead leading from the nature of the protocol and does not include coding overhead. Therefore, Table 1 provides an overview of available code rates of each IoT protocol and the maximum achievable payload ratio $R_{p,max}$ when transmitting the maximum amount of user payload p_{max} in bytes. Most IoT protocols use a fixed code rate of either 1/2 or 1/3 with exception to LoRa and LR-FHSS. For further understanding, the visualization in Figure 6 compares the overhead lengths of the protocols, including coding overhead and redundancy through header or packet replicas.

In Figure 7, we extend the graph from Figure 5 with the target of transmitting up to 500 bits of user payload. As a consequence, multiple packets need to be sent to transport the entire payload depending on the design of the IoT protocol. In Figure 7, newly initialized packets can be identified by a drop in the payload ratio; at these points, fixed header sizes contribute significantly to the overhead and thus reduce efficiency. We recognize the highest efficiency drops with the beginning of the second packet. As more packets are needed to transmit a chosen payload, the less significant are the efficiency drops of the added packet overhead.

4.2 | Comparison of Effective Spectral Efficiency

For a more profound insight into transmission differences of the protocols, we performed a comparison based on the protocols spectral efficiency. Originating from a respective literature review, we could identify the following publications which provide information about data throughput and performance of the protocols LoRa (DR0, SF12) [67], Figure 4, LR-FHSS (DR8) [67], Figure 4, TS-UNB ($k = 200$) [68], Figure 13, UCSS ($\sigma = 0dB$) [54], Figure 15, and E-SSA (without preamble searcher) [69], Figure 17. Note that, to the best of our knowledge,

we have not identified a respective publication on throughput performance of Sigfox so far. The published data were adapted to the metric of spectral efficiency and case-dependent adjusted toward the real user payload accordingly, as introduced in (4). Hence, Figure 8 presents the effective received throughput in user-bits/s/Hz as a function of the transmit traffic load likewise in user-bits/s/Hz. The dashed line P_{succ} represents the ideal case, when each transmitted user-bit is correctly received.

It is observed from the figure that E-SSA, UCSS, and TS-UNB provide the best spectral efficiencies with respect to user bits. However, an assessment of applicability in an IoT use case requires additional technical knowledge on energy consumption to successfully close the link between device and satellite. The following section extends our comparison to an application within the presented MaReBa IoT scenario.

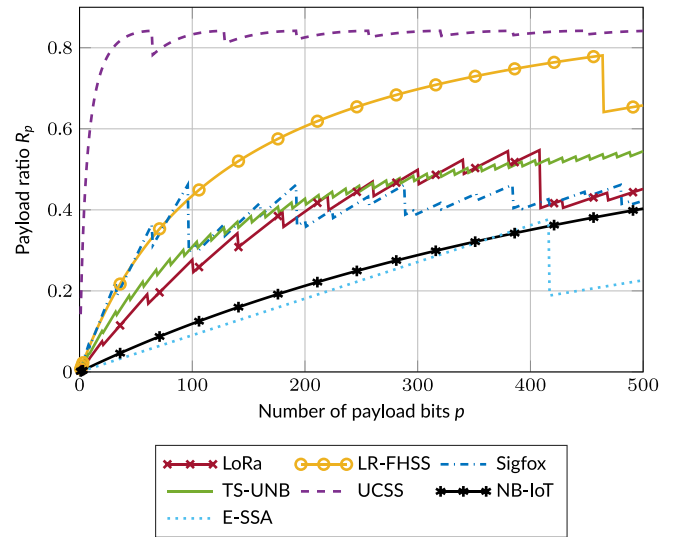


FIGURE 7 | Portion of user bits per packet (payload ratio) $R_{p,n}$ as a function of payload size regarding protocol specific maximum user payload leading to multiple packet transmissions.

LoRa									
Pre 12 sb	PHDR Hdr 56	MH DR 16	FHDR 112	FPort 16	User Payload	MIC 64	CRC 32		
LR-FHSS									
SyncWord 96		PHDR 192			PHDR CRC 48	User Payload	CRC 48		
Sigfox									
Preamble 57	FT 39	MAC Hdr 144			User Payload	Auth 48 to 120	CRC 48		
TS-UNB									
PHY Hdr 108		MAC Hdr 36	Addr 72	MPDUCNT 108	MPF 0 to 36	User Payload	Sign 144	MIMode	Tail 27
E-SSA									
Preamble 128		UW 36	PDRACH Hdr 192			User Payload	CRC 48	fill 12	
Preamble 128		PCRACH Frame total 1536 (not scaled)							
UCSS									
P 6	Pau 13	User Payload	CRC 16						

FIGURE 6 | Comparison of satellite IoT protocol structures with focus on the overhead drawn in scale. Lengths are specified in coded bits including redundancy through packet/header replicas. User data are set to 40 bits but can be extended to the protocol-specific limits which do not contribute to comparability here.

4.3 | Comparison of Energy per Information Bit

A fair comparison of IoT protocols for a battery-powered IoT scenario should involve the evaluation of the energy required to transmit a user bit. As a metric, we use the E_{ib}/N_0 value introduced in (12), calculated from simulation and measurement parameters of corresponding publications. We integrate the previously established link budget to compute back from the known required E_b/N_0 at the satellite to the EIRP needed at the IoT device. We assume a common user data rate of 100 user-bit/s for all protocols, yielding the bandwidth of the protocol-specific used spectrum under consideration of payload ratio, modulation order, and spreading factor. For estimation of the required EIRP at the transmitter that incorporates the link budget, we consider three different clear-sky satellite scenarios according to the parameters listed in Table 2.

For the space segment, we assume circular polarized VHF/UHF antennas [70, 71] with 0dBi gain for the LEO and a fixed 12dBi gain for the GEO that covers the surface of the earth with the antenna from its point of view. For the IoT transceiver on the ground, we assume a 0-dBi gain antenna with linear polarization and almost omnidirectional characteristic. Thus, the polarization loss contributes with 3dB [72].

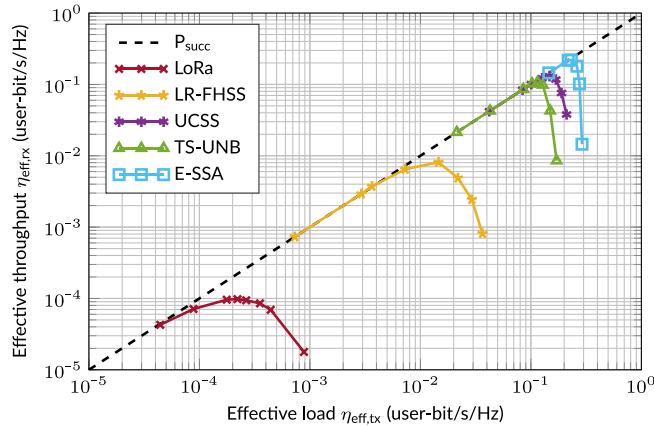


FIGURE 8 | Comparison of spectral efficiencies yielding from the received effective throughput as function of the effective transmitted load in user-bit/s/Hz of selected satellite IoT protocols.

TABLE 2 | Link budget parameters and assumptions.

		LEO best	LEO worst	GEO
Elevation ϵ	deg	90	10	34
Altitude a	km	400	400	35786
Carrier frequency f_c	MHz	868	868	868
Sat. antenna gain G_s	dBi	0	0	12
FSPL L_{fspl}	dB	143.3	154.4	182.9
Attenuation L_{att}	dB		3	
Noise temperature T_{noise}	K		290	

Rain attenuation is not considered for the clear-sky scenario. Likewise, pointing losses are not taken into account similar to the setting in [39].

For LoRa, the parameters are used at the highest spreading factor ($n_{SF} = 12$) and -20 dB required SNR at the receiver as officially stated by Semtech [73]. Regarding TS-UNB, we extract from Kilian et al. [68], Figure 11 a required E_b/N_0 of about 7.6dB considering a channel load of 0.2 and 10^{-4} telegram error probability. For the UCSS waveform, we choose the US-6 measurement configuration from Hofmann et al. [56], Table 1 with a required SNR of -20 dB. For E-SSA [69], an E_b/N_0 value of 10.8 dB for a packet error rate of 10^{-3} can be calculated considering a spreading factor of 16. Based on this, we calculate an estimate of the effective energy efficiency defined in (14). If multiple data sources were available, we always selected protocol and waveform configurations leading to the most fairly comparison. The LR-FHSS protocol is not included in the comparison, as the publication base is very scarce and not sufficient information is available for a fair comparison. Similar for the protocol Sigfox, the proprietary nature of the protocol is the main reason for the scarcity of information.

Table 3 compiles all parameters and presents resulting calculations for the three mentioned satellite scenarios and an added comparison of the LEO best case with equal payload length. Observing the E_{ib}/N_0 , we recognize the high influence of the protocol overhead on the energy per user-bit, required to close the satellite link for transmitting the user payload. The influence of a maximum chosen payload can be seen in the comparison with the equal-payload (64 bit) scenario in the bottom section of the table. Filling the total available user payload of a protocol is necessary to ensure the optimal payload ratio for the highest energy efficiency.

Further, we recognize the consequential increase in required P_{eirp} for closing the link from LEO best case to GEO. Likewise, the effective energy efficiency in number of carried user-bits per Joule decreases accordingly. In total, the effective energy efficiency of UCSS outperforms the remaining protocols due to its high payload ratio, followed by TS-UNB which instead starts with a better E_b/N_0 into the calculation. The remaining two protocols rank with similar energy efficiencies behind the mentioned ones.

TABLE 3 | Energy comparison in clear-sky conditions of LEO best case (90° el.), LEO worst case (10° el.), and GEO.

Source		LoRa [56]	TS-UNB [68]	UCSS [56]	E-SSA [69]
Mod		CSS/FSK	BPSK	DBPSK	BPSK
Mod order	bit/symb	12	1	1	1
R_{ib}	user-bit/s	100	100	100	100
R_c		1/2	1/3	1/2	1/3
Spreading		4096	1	373	16
B	kHz	385.7	0.7	88.6	12.7
Γ	dB	-20	2.8	-19.2	-6
E_b/N_0	dB	8.3	7.6	9.5	10.8
p_{src}	bit	64	200	64	416
$R_p(p_{src})$		0.177	0.427	0.842	0.378
E_{ib}/N_0	dB	15.9	11.3	10.2	15.0
LEO best case (400km alt., 90° el.):					
P_{eirp}	dBW	-21.9	-26.4	-27.5	-22.7
ξ_{eff}	user-bit/J	15344	43954	55902	18553
LEO worst Case (400km alt., 10° el.):					
P_{eirp}	dBW	-10.7	-15.3	-16.4	-11.6
ξ_{eff}	user-bit/J	1185	3394	4317	1433
GEO (34.2° el.):					
P_{eirp}	dBW	5.8	1.2	0.1	4.9
ξ_{eff}	user-bit/J	27	76	97	32
LEO best case (400km alt., 90° el.)- Equal payload per protocol:					
p_{eq}	bit	64	64	64	64
$R_p(p_{eq})$		0.177	0.237	0.842	0.058
E_{ib}/N_0	dB	15.9	13.9	10.2	23.2
P_{eirp}	dBW	-21.9	-23.9	-27.5	-14.5
ξ_{eff}	user-bit/J	15344	24373	55902	2842

5 | Massive Multiple Access Very Low Power Wide Area Networks

In this paper, we analyzed LPWAN protocols for satellite communications. With respect to other protocols, they provide comparatively low data rates at a higher range as shown in Figure 9. There, terrestrial IoT protocols with ranges typical for industrial utilization are grouped in the dashed box. It is distinguished between those being part of the 3GPP standardization as NB-IoT and LTE-M and those originating from a community-based, respectively, proprietary implementation of a communication protocol stack as for example LoRa and Sigfox. Since some terrestrial LPWAN protocols are currently discussed for application in satellite IoT, these were grouped in the red box on the right side of the figure indicating the higher range capability.

In the preceding section, we compared the suitability of the presented protocols in satellite IoT through a step-by-step analysis based on the introduced efficiency criteria, namely, the protocol overhead, the effective spectral efficiency, and the effective energy efficiency. The comparison showed in Table 3 that the effective energy efficiency in user-bit/J varies between 2.8 and 55.9kbit J⁻¹ for very short but equal payload lengths in the best case LEO scenario. Due to their individual structural design, the protocols under investigation suit differently well for applications with very short payloads. Consequently, the amount of protocol overhead and coding has a high impact on the efficiency of a particular protocol.

With the MaReBa scenario, we created an application case that implies specific requirements on the underlying IoT technology to ultimately support a large number of battery-powered,

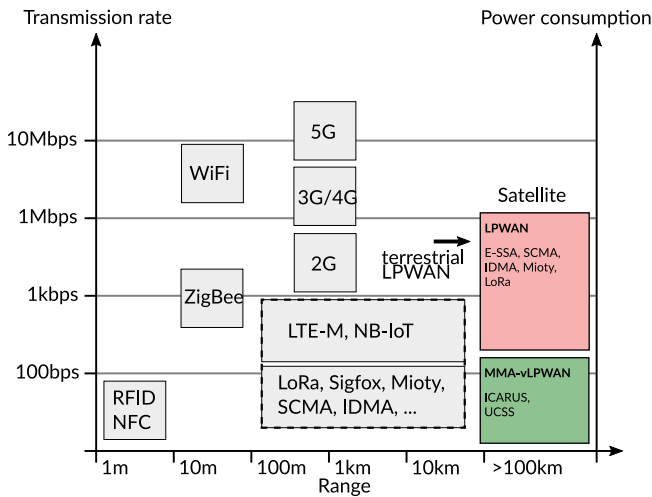


FIGURE 9 | Embedding of MMA-vLPWAN as a new class of IoT technologies in the spectrum of range and data throughput.

satellite-connected IoT devices. Finally, we propose to summarize those protocols suited for the MaReBa scenario that perform highly energy-efficient via satellite at very short message lengths in a novel class named MMA-vLPWAN. The class is shown in the lower right of Figure 9, which indicates lower transmit rates and lower power consumption compared to standard LPWAN.

Based on four comparison criteria with respect to the MaReBa scenario, Figure 10 visualizes the gap that is occupied by the waveforms of the new IoT class MMA-vLPWAN within a radar chart. We selected the following criteria: energy per bit, EIRP, inverse spectral efficiency, and weight, respectively, size of the IoT device. For the classification of weight and size of suitable terminals, we orient on public information about dimensions of existing devices and terminals. Furthermore, the average values of EIRP and energy per bit also provide information about approximate dimensions of the user terminal, since both variables have influence on the installed battery size.

The most of the previously discussed technologies and standards tend to locate on the outer area of the diagram. According to the graph design, this means a mediocre to poor performance with regard to the characteristics of the MaReBa IoT scenario. Representatives of MMA-vLPWAN, instead, locate in the center of the radar chart in Figure 10 and score a low value on all axes. UCSS, a dedicated satellite IoT waveform, has already demonstrated the capability of GEO connectivity [54] and has scored very good results in the energy efficiency comparison. Further, the transmission technology of the previously mentioned ICARUS animal tracking system is counted toward MMA-vLPWAN, since the miniature transmitters attached to a variety of animals communicating via the space segment on ISS, symbolize the technical demands that MMA-vLPWAN technologies have to cope with [66]. At its time, the ICARUS waveform was a ground-breaking technology that first introduced MMA-vLPWAN communication capability. Since it is not a commercial standard, we did not include it in the previous comparison. This also applies to the SCMA/IDMA-based technologies; however, they may also fit as candidates for the MMA-vLPWAN

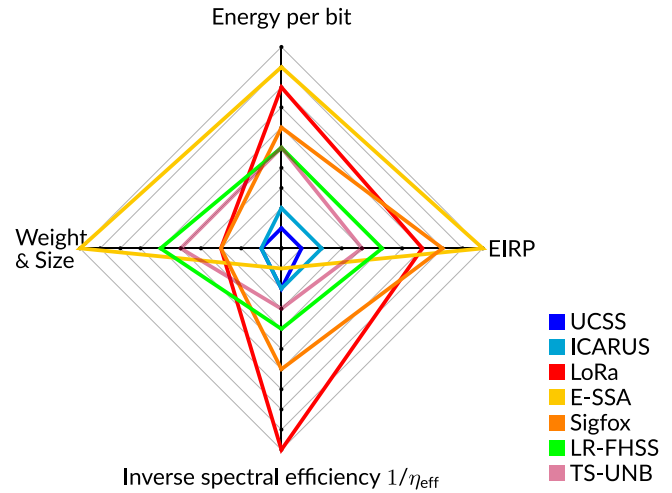


FIGURE 10 | Categorical integration of MMA-vLPWAN in the broad field of satellite IoT. Technologies as UCSS and ICARUS cover the gap of highly energy and bandwidth efficient protocols with low EIRP and weight characteristics. Values of the radar chart go from low (center) to high (outside).

class [74]. Ultimately, the classification of MMA-vLPWAN protocols brings an important contribution to the overall understanding of the field of satellite IoT, which consequently results in greater transparency and comprehensibility for industrial implementation.

6 | Conclusion and Future Work

In this paper, we identified the critical need for a thorough examination of protocols and waveforms for direct-to-satellite IoT applications, particularly under stringent energy constraints such as battery usage. We addressed this by developing a comprehensive analytical framework to compare the most promising IoT protocols in the satellite IoT domain. A novel evaluation metric, which accounts for protocol overhead, was proposed and applied. Our extensive analysis included considerations of overhead, spectral efficiency, and energy efficiency, revealing the significant impact of protocol-specific overhead on the overall energy consumption for transmitting a fixed user payload length. Additionally, our findings highlighted that protocols achieve optimal performance with full utilization of the maximum available payload size. However, differences in performance due to the design of the underlying PHY layer technology offer valuable insights for more efficient, case-specific protocol applications.

The recent advancements in satellite IoT have been significantly influenced by the cost-effective rocket launch capabilities of the New Space movement, leading to the deployment of the first prototype satellites. Consequently, the focus is now shifting toward the system optimization of future satellite fleets. A key aspect of this optimization is to incorporate energy efficiency considerations into the design stage of new satellite IoT transmission technologies, ensuring their successful application in MaReBa IoT scenarios. In this context, the development of new satellite IoT protocols that can support a long operating lifetime for battery-powered IoT devices has led to the introduction of the

MMA-vLPWAN IoT class. Future research will aim to integrate hardware-related energy consumption considerations, including transmitter and receiver design, latency estimation, satellite system architecture, uplink multiple access overhead, and downlink communication strategies for battery-powered IoT devices.

References

1. "Ericsson Mobility Report," Ericsson, (Stockholm, Sweden, 2023).
2. F. Grijpink, E. Kutcher, A. Ménard, et al., "Connected World: An Evolution in Connectivity Beyond the 5G Revolution," McKinsey Global Institute, (2020).
3. X. Lin, S. Rommer, S. Euler, E. A. Yavuz, and R. S. Karlsson, "5g from SPACE: An Overview of 3GPP Non-Terrestrial Networks," *IEEE Communications Standards Magazine* 5, no. 4 (2021): 147–153.
4. L. Zhang, Y.-C. Liang, and D. Niyato, "6g Visions: Mobile Ultra-Broadband, Super Internet-of-Things, and Artificial Intelligence," *China Communications* 16, no. 8 (2019): 1–14.
5. W. Jiang, B. Han, M. A. Habibi, and H. D. Schotten, "The Road Towards 6G: A Comprehensive Survey," *IEEE Open Journal of the Communications Society* 2 (2021): 334–366.
6. N. Pachler, I. del Portillo, E. F. Crawley, and B. G. Cameron, "An Updated Comparison of Four Low Earth Orbit Satellite Constellation Systems to Provide Global Broadband," in *2021 IEEE International Conference on Communications Workshops (ICC Workshops)*, (2021): 1–7.
7. C. Daehnick, I. Klinghoffer, B. Maritz, and B. Wiseman, "Large LEO Satellite Constellations: Will It Be Different This Time?," (2020), Accessed: 2023-11-21.
8. Apple, "Emergency SOS Via Satellite on iPhone 14 and iPhone 14 Pro Lineups Made Possible by \$450 Million Apple Investment in US Infrastructure," (2022), Accessed: 2023-11-21.
9. T-Mobile US Media Relations, "T-Mobile Takes Coverage Above and Beyond With SpaceX," (2022), Accessed: 2023-11-20.
10. Vodafone, "Vodafone and AST SpaceMobile Unveil Launch Plans for Space-Based Mobile Network Initially Reaching 1.6 Billion People," (2020), Accessed: 2023-11-21.
11. Qualcomm, "Qualcomm Introduces Snapdragon Satellite, The World's First Satellite-Based Solution Capable of Supporting Two-Way Messaging for Premium Smartphones and Beyond," (2023), Accessed: 2024-03-11.
12. E. Kulu, "Satellite Constellations - 2021 Industry Survey and Trends," in *35th Annual Small Satellite Conference*, (2021).
13. A. Curry, "The Internet of Animals That Could Help To Save Vanishing Wildlife," *Nature* 562, no. 7727 (2018): 322–326.
14. W. Jetz, G. Tertitski, R. Kays, et al., "Biological Earth Observation With Animal Sensors," *Trends in Ecology & Evolution* 37, no. 4 (2022): 293–298.
15. K. G. Andersen, A. Rambaut, W. I. Lipkin, E. C. Holmes, and R. F. Garry, "The Proximal Origin of SARS-CoV-2," *Nature Medicine* 26, no. 4 (2020): 450–452.
16. M. De Sanctis, E. Cianca, G. Araniti, I. Bisio, and R. Prasad, "Satellite Communications Supporting Internet of Remote Things," *IEEE Internet of Things Journal* 3, no. 1 (2016): 113–123.
17. M. Harris, "Swarm Wants to Send Hundreds of Tiny CubeSats Into Orbit," (2019), Accessed: 2024-03-12.
18. C. Henry, "Australian IoT Startup Myriota Raises \$19 Million," (2020), Accessed: 2024-03-12.
19. E. HooperLee, "The Astrocast Nanosatellite IoT Network Goes Live," (2021), Accessed: 2024-03-12.
20. A. R. Wilson, "Estimating the CO2 Intensity of the Space Sector," *Nature Astronomy* 6, no. 4 (2022): 417–418.
21. C. M. Maloney, R. W. Portmann, M. N. Ross, and K. H. Rosenlof, "The Climate and Ozone Impacts of Black Carbon Emissions From Global Rocket Launches," *Journal of Geophysical Research: Atmospheres* 127, no. 12 (2022): 1–17.
22. H. Huang, S. Guo, W. Liang, K. Wang, and A. Y. Zomaya, "Green Data-Collection From Geo-Distributed IoT Networks Through Low-Earth-Orbit Satellites," *IEEE Transactions on Green Communications and Networking* 3, no. 3 (2019): 806–816.
23. J. A. Fraire, G. Nies, C. Gerstacker, H. Hermanns, K. Bay, and M. Bisgaard, "Battery-Aware Contact Plan Design for LEO Satellite Constellations: The Ulloriaq Case Study," *IEEE Transactions on Green Communications and Networking* 4, no. 1 (2020): 236–245.
24. M. Krondorf, S. Bittner, D. Plettemeier, A. Knopp, and M. Wikelski, "ICARUS – Very Low Power Satellite-Based IoT," *Sensors* 22, no. 17 (2022): 6329.
25. L. Ouvry, D. Lachartre, C. Bernier, F. Lepin, F. Dehmas, and V. Deslandes, "An Ultra-Low-Power 4.7mA-Rx 22.4mA-Tx Transceiver Circuit in 65-nm CMOS for M2M Satellite Communications," *IEEE Transactions on Circuits and Systems II: Express Briefs* 65, no. 5 (2018): 592–596.
26. M. Centenaro, C. E. Costa, F. Granelli, C. Sacchi, and L. Vangelista, "A Survey on Technologies, Standards and Open Challenges in Satellite IoT," *IEEE Communications Surveys & Tutorials* 99 (2021): 1–1.
27. Z. Qu, G. Zhang, H. Cao, and J. Xie, "LEO Satellite Constellation for Internet of Things," *IEEE Access* 5 (2017): 18391–18401.
28. R. De Gaudenzi, O. Del Rio Herrero, G. Gallinaro, S. Cioni, and P.-D. Arapoglou, "Random Access Schemes for Satellite Networks, From VSAT to M2M: A Survey," *International Journal of Satellite Communications and Networking* 36, no. 1 (2018): 66–107.
29. T. Ferrer, S. Céspedes, and A. Becerra, "Review and Evaluation of MAC Protocols for Satellite IoT Systems Using Nanosatellites," *Sensors* 19, no. 8 (2019): 1947.
30. O. Kodheli, E. Lagunas, N. Maturo, et al., "Satellite Communications in the New Space Era: A Survey and Future Challenges," *IEEE Communications Surveys & Tutorials* 23 (2020): 70–109.
31. R. Birkeland and D. Palma, "An Assessment of IoT Via Satellite: Technologies, Services and Possibilities," in *Proceedings of the International Astronautical Congress, IAC*, Vol. 2019-October, (2019).
32. M. Koziol, "Satellites Can Be a Surprisingly Great Option for IoT," (2021), Accessed: 2024-03-13.
33. J. M. Gongora-Torres, C. Vargas-Rosales, A. Aragon-Zavala, and R. Villalpando-Hernandez, "Link Budget Analysis for LEO Satellites Based on the Statistics of the Elevation Angle," *IEEE Access* 10 (2022): 14518–14528.
34. H. M. Kwon and T. Birdsall, "Channel Capacity in Bits per Joule," *IEEE Journal of Oceanic Engineering* 11, no. 1 (1986): 97–99.
35. E. Bjornson and E. G. Larsson, "How Energy-Efficient Can a Wireless Communication System Become?," in *2018 52nd Asilomar Conference on Signals, Systems, and Computers*, Vol. 2018-October, (IEEE, 2018): 1252–1256.
36. A. Augustin, J. Yi, T. Clausen, and W. M. Townsley, "A Study of LoRa: Long Range and Low Power Networks for the Internet of Things," *Sensors* 16, no. 9 (2016): 1466.
37. T. Wu, D. Qu, and G. Zhang, "Research on LoRa Adaptability in the LEO Satellites Internet of Things," in *2019 15th International Wireless Communications & Mobile Computing Conference (IWCMC)*, (IEEE, 2019): 131–135.

38. G. Alvarez, J. A. Fraire, K. A. Hassan, S. Cespedes, and D. Pesch, "Uplink Transmission Policies for LoRa-Based Direct-to-Satellite IoT," *IEEE Access* 10, no. June (2022): 72687–72701.
39. L. Fernandez, J. A. Ruiz-De-Azua, A. Calveras, and A. Camps, "Assessing LoRa for Satellite-to-Earth Communications Considering the Impact of Ionospheric Scintillation," *IEEE Access* 8 (2020): 165570–165582.
40. Semtech Corporation, "Datasheet SX1276/77/78/79," (2020), May.
41. LoRa™ Alliance, "RP002-1.0.1 LoRaWAN - Regional Parameters," (2020), LoRaWAN - RP002-1.0.1, 1–88.
42. LoRa Alliance, "RP2-1.0.2 LoRaWAN® Regional Parameters," (2020), 94.
43. M. A. Ullah, G. S. Member, K. Mikhaylov, and S. Member, "Analysis and Simulation of LoRaWAN LR-FHSS for Direct-to-Satellite Scenario," *IEEE Wireless Communications Letters* 11, no. 3 (2022): 548–552.
44. Sigfox, "Website Sigfox," (2023), Accessed: 2024-03-19.
45. Sigfox, "Plastimo and Sigfox Join Forces to Connect the Oceans," (2019), Accessed: 2024-03-19.
46. Sigfox, "Sigfox Connected Objects: Radio Specifications April 2023," (2023), Accessed: 2024-03-19.
47. Fraunhofer IIS, "mioty® – Drahtlose LPWAN Technologie," (Nürnberg: Fraunhofer-Institut für Integrierte Schaltungen IIS, 2024), Accessed: 2024-03-19.
48. Fraunhofer IIS, "Fraunhofer IIS Successfully Tests Terrestrial IoT Technology Mioty® via GEO Satellite," (2021), Accessed: 2024-03-19.
49. ETSI, "TS 103 357 - V1.1.1 - Short Range Devices; Low Throughput Networks (LTN); Protocols for Radio Interface A," *European Telecommunications Standards Institute* 1 (2018): 1–113.
50. Mioty Alliance, "Connect at Scale," (2023), Accessed: 2024-06-04.
51. ETSI, "TS 102 721-4 - V1.1.1 - Satellite Earth Stations and Systems; Air Interface for S-band Mobile Interactive Multimedia (S-MIM); Part 4: Physical Layer Specification, Return Link Synchronous Access," (2011), European Telecommunications Standards Institute (ETSI), 1.
52. O. Del Rio Herrero and R. De Gaudenzi, "High Efficiency Satellite Multiple Access Scheme for Machine-to-Machine Communications," *IEEE Transactions on Aerospace and Electronic Systems* 48, no. 4 (2012): 2961–2989.
53. O. del Rio Herrero and R. De Gaudenzi, "Method, Apparatuses and System for Asynchronous Spread-Spectrum Communication," (2011), 2, 12.
54. C. A. Hofmann and A. Knopp, "Ultrararrowband Waveform for IoT Direct Random Multiple Access to GEO Satellites," *IEEE Internet of Things Journal* 6, no. 6 (2019): 10134–10149.
55. A. Knopp, C. Hofmann, and R. Schwarz, *Orthogonal Correlation Signals for Detection and Synchronization at Low SNR* (Germany: Neubiberg, 2021).
56. C. A. Hofmann, K. U. Storek, and A. Knopp, "Impact of Phase Noise and Oscillator Stability on Ultra-Narrow-Band-IoT Waveforms for Satellite," in *IEEE International Conference on Communications*, (2021).
57. M. Kanj, V. Savaux, and M. Le Guen, "A Tutorial on NB-IOT Physical Layer Design," *IEEE Communications Surveys & Tutorials* 22, no. 4 (2020): 2408–2446.
58. 3GPP, "Evolved Universal Terrestrial Radio Access (E-UTRA); Technical Specification Group Radio Access Network; Multiplexing and Channel Coding," 36.212. 3rd Generation Partnership Project (3GPP), (2023), Version 18.0.0.
59. H. Chougrani, S. Kisseleff, W. A. Martins, and S. Chatzinotas, "NB-IOT Random Access for Nonterrestrial Networks: Preamble Detection and Uplink Synchronization," *IEEE Internet of Things Journal* 9, no. 16 (2022): 14913–14927.
60. C. Yang, M. Wang, L. Zheng, and G. Zhou, "Folded Chirp-Rate Shift Keying Modulation for LEO Satellite IoT," *IEEE Access* 7 (2019): 99451–99461.
61. T. Myers and M. Hughes, "System and Method for Compensating the Effects of Doppler," (2020).
62. T. Myers and A. Viterbi, "Doppler Multi-Channel Spread Spectrum (DMSS) to Serve the Massive Asset Tracking and Monitoring Market," Totum Labs, (2019).
63. Totum Labs, "Totum Achieves World's First Indoor, Direct-to-Satellite IoT Connection, Books 2 Million Advance Orders," (2021), Accessed: 2024-03-22.
64. R. J. F. Fang, M. Eroz, and N. Becker, "Data collection and SCADA Over GEO-MSS Satellites Using Spread SCMA," in *2009 International Workshop on Satellite and Space Communications*, (IEEE, 2009): 441–445.
65. L.-N. Lee, M. Eroz, L. Chen, and R. Gopal, "Scrambled Code Multiple Access Waveform for Micro Satellite Terminals," in *Milcom 2012 - 2012 IEEE Military Communications Conference*, (IEEE, 2012): 1–6.
66. M. Krondorf, "The Internet of Animals," *Rohde & Schwarz News Magazine Nr. 219* (2018): 64–68.
67. G. Boquet, P. Tuset-Peiro, F. Adelantado, T. Watteyne, and X. Vilajosana, "LR-FHSS: Overview and Performance Analysis," *IEEE Communications Magazine* 59, no. 3 (2021): 30–36.
68. G. Kilian, M. Breiling, H. H. Petkov, et al., "Increasing Transmission Reliability for Telemetry Systems Using Telegram Splitting," *IEEE Transactions on Communications* 63, no. 3 (2015): 949–961.
69. A. Arcidiacono, D. Finocchiaro, R. De Gaudenzi, et al., "Is Satellite Ahead of Terrestrial in Deploying NOMA for Massive Machine-Type Communications?," *Sensors* 21, no. 13 (2021): 4290.
70. EnduroSat, "UHF Antenna 2U," (2023), Accessed: 2024-03-24.
71. Innovative Solutions in Space, "Antenna Systems," (2016), Accessed: 2024-03-24.
72. G. Sciddurlo, A. Petrosino, M. Quadri, et al., "Looking at NB-IoT Over LEO Satellite Systems: Design and Evaluation of a Service-Oriented Solution," *IEEE Internet of Things Journal* 9 (2021): 14952–14964.
73. Semtech Corporation, "LoRaWAN – Simple Rate Adaptation Recommended Algorithm," (2016), 1–8.
74. L.-N. Lee, M. Eroz, N. Becker, et al., "Scrambled Coded Multiple Access, Variations and Improvements," in *2018 IEEE Global Communications Conference (GLOBECOM)*, (IEEE, 2018): 1–7.